Soft Matter

PAPER

Cite this: *Soft Matter*, 2015, **11**, 169

Velocimetry in microchannels using photobleached molecular tracers: a tool to discriminate solvent velocity in flows of suspensions

Florinda Schembri,† Hugues Bodiguel* and Annie Colin

Received 12th September 2014
Accepted 22nd October 2014

DOI: 10.1039/c4sm02049a

www.rsc.org/softmatter

We report the development and analysis of a velocimetry technique based on the short time displacement of molecular tracers, tagged thanks to photobleaching. We use confocal microscopy to achieve a good resolution transverse to the observation field in the direction of the velocity gradient. The intensity profiles are fitted by an approximate analytical model which accounts for hydrodynamic dispersion, and allow access to the local velocity. The method is validated using pressure driven flow in microfluidic slits having a thickness of a few tens of micrometers. We discuss the main drawbacks of this technique which is an overestimation of the velocity close to the walls due to the combination of molecular diffusion and shear. We demonstrate that this error, limited to a near wall region of a few micrometers thick, could be controlled by limiting the diffusion of fluorophore molecules or minimizing the bleaching time. The presented technique could be combined with standard particle imaging velocimetry to access velocity differences and allow particle trajectory analysis in microflows of suspensions.

1 Introduction

A suspension is a system where particles are dispersed throughout a solvent.[1] These systems are ubiquitous in nature and are encountered in many areas ranging from cement and concrete technology, ceramic processing, coating and pigment technology, propellants and explosive science, mineral processing, soil science, composite processing and various slurry flow technologies. Precise predictive models of flow of such complex fluids are crucial in many applications from food to aeronautical industry. Accurate simulation of suspension flows is a crucial enabler for industrial process optimization. Composite material fabrication, propergol paste into a mould, injection or ejection of suspensions through nozzles in biomedical practice represent archetypical applications. In all these applications, suspensions are submitted to flow. Hence the rheology of suspensions is the object of intense research from the theoretical, experimental and numerical points of view. In this area, a well-known and long-standing problem in fluid mechanics has been the calculation of the effective viscosity of a suspension. The dilute and semi-dilute regimes have been well understood since the pioneering studies of Einstein (1905) and Batchelor and Green (1972). In the past decades, many studies have been focused on the concentrated regime where the average distance between the particles is less than the mean size of a particle. As suggested by dimensional analysis and confirmed by numerical simulations and experiments, dense suspensions of hard spheres are Newtonian: the shear stress is proportional to the shear rate. However, in this regime shocks between particles and short-range forces give rise to concentration inhomogeneities[2] that may be misinterpreted as non-Newtonian effects. Indeed, numerous authors reported experimental data of relative suspension viscosity apparently showing shear rate dependence. Nevertheless, Ovarlez *et al.*[3] showed that this phenomenon is rather related to a heterogeneous distribution of the particle concentration in the rheometer. Understanding the flow of a dispersion requires thus to address the question of the particle migration and of the building of concentration heterogeneities. The migration flux is directly related to the difference between liquid and particle velocities.[4] At this stage, the simultaneous measurement of both velocities in the flow direction has never been performed. In this article, we display an experimental setup allowing such a characterization of the flow.

Particle velocity is classically measured using micro-particle tracking velocimetry (PTV). This technique is widely used as it allows acquiring, with a great resolution time and space, resolved velocity profiles.[5–7] The sample is illuminated so that the particles are visible. A camera records their movements. The analysis of the movies involves two basic steps. The first is segmentation, in which multiple particles in a field of view are identified and discriminated. Subsequently, an algorithm tracks the particles individually to monitor their displacement between successive video frames.[8] Tracking algorithms used to

Univ. Bordeaux, CNRS, Solvay, LOF UMR 5258, France. E-mail: hugues.bodiguel@u-bordeaux.fr

† Present address: Laboratoire Photonique, Numérique et Nanosciences (LP2N) UMR 5298, CNRS – IOGS – Université Bordeaux, Institut d'Optique d'Aquitaine 33400 Talence, France.

date have included cross-correlation of subsequent images,[9] calculation of the center-of-mass (centroid) of the object of interest[10] and direct Gaussian fits to the intensity profile.[11] Some groups have claimed nanometer resolution.

The solvent measurement velocity is less developed. The use of molecular tracers has been proposed in previous studies (see ref. 12 for a review of a pioneer study). Caged-fluorescent dye molecules have proven to be very powerful[13,14] but require the use of UV-light (and consequently adequate materials for device fabrications) and expensive sensors. In contrast, photobleaching of fluorescent dyes uses visible wavelengths and moreover it is a standard option in confocal microscopy equipments.

Two main strategies have been developed to take advantage of photobleaching to measure flow velocities. The first one is based on the fact that the fluorescence intensity under a given illumination monotonically increases with the flow velocity. This technique, designed as laser induced fluorescence photobleaching anemometry (LIFPA),[15,16] has been extended to single-point measurements[17] allowing the determination of velocity profiles. Successively, the same group showed that it can be coupled with stimulated emission depletion (STED) microscopy in order to achieve a spatial resolution below the micron scale.[18] The main drawback of this method is the need of light intensity calibration prior to the measurements. One can thus anticipate that, although very powerful for some applications, this drawback could limit its use with heterogeneous and complex fluids.

The second class of the molecular tracer velocimetry (MTV) techniques based on photobleaching take advantage of direct spatial measurement of the displacement of a photobleached region in the flow[19–24] with a bright fluorescent background. It is thus similar to the principle of μ-PIV, but with tagged molecules as tracers. The disadvantage of such a size reduction is an increase of tracer diffusivity, which rapidly broadens the band created by the laser. To overcome this issue, Molho *et al.*[19] and Mosier *et al.*[20] used fluorescein grafted on macromolecules to reduce its diffusivity. Furthermore, the use of macromolecular probes suffers from similar limitations to particle probes. Nevertheless, hydrodynamic dispersion remains an important drawback and it has been concluded that it was better adapted to electroosmotic flows than pressure-driven ones. In the work of Cuenca and Bodiguel,[22] it was shown that a small fluorescent molecule could be used even in the Taylor–Aris dispersion regime, focusing on a very short time regime just after the bleaching. This study was devoted to very thin channels, so that the velocity field along the thickness was averaged. A method was proposed in recent studies of Ponjavic *et al.*[23] and of Wexler *et al.*[24] to obtain information on the velocity field in the transverse direction, based on the fact that the dispersion of the photobleached spot is strongly related to the velocity gradients. However, this approach is only valid where the features of transverse velocity profiles are known, as it only gives access to the global shear rate.

In this work, we show that 2D-velocimetry is possible using photobleaching based MTV, with a spatial resolution on the order of a few micrometers, and with small molecular dyes. The idea is very simple since it takes advantage of confocal microscopy to achieve the required resolution in the vorticity direction. We focus on short times following a bleached region of fluid, similar to ref. 22, in order to reduce dispersion and diffusion issues. The main advantage of this technique is the use of molecular tracers. Moreover the presented technique does not require any calibration. We explain in the following that due to the short time limit required, a detailed analysis of the intensity curves is often necessary. Then, we validate the measurement in Poiseuille flow, and discuss the systematic error occurring in the near-wall region. Finally, we propose an application of the technique to the velocity calculation of both fluids and particles in semi-dilute and dense regimes for suspensions of hard spheres, by combining our technique with μ-PTV.

2 Experimental details

Confocal photobleaching velocimetry is developed and validated using pressure driven flows in microchannels. Since we only focus here on 2D velocimetry, we use microchannels having a large aspect ratio, as depicted in Fig. 1: the channel width is ten times the height. Two microchannels are used, of heights 50 and 100 μm, and of length 100 mm. They are fabricated in borosilicate and were purchased from Vitrocom. The inlet and outlet of the capillary are directly immersed in a plastic reservoir of controlled pressure, set using a pressure-control regulator (MFCS 4C, Fluigent). This simple setup allows us to impose a well defined and stable pressure gradient, with an accuracy smaller than 1%.

The capillary is placed just above a Zeiss LSM 5 inverted confocal microscope, with an oil immersion 40× objective of numerical aperture 1.3. In full resolution, the imaging frequency is limited to 60 frames per second. The pinhole aperture has been set at its minimum (1 μm). The same laser ($\lambda = 488$ nm) is used to bleach and image the flow. During the bleaching step, the laser power is set at its maximum (100 mW)

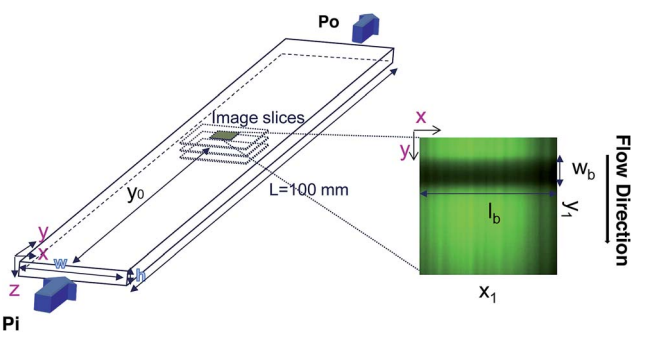

Fig. 1 Scheme of the microflow device used in the experiments. Two rectangular borosilicate capillaries of $h_1 = 50$ μm, $w_1 = 500$ μm and $h_2 = 100$ μm, $w_2 = 1000$ μm cross-sections are used. Their length is equal to $L = 100$ mm. The flow is pressure driven and imaged at 60 frames per second. The fluid is photobleached in a rectangular region, perpendicular to the flow gradient, of fixed length $l_b = 106.63$ μm and of width w_b varying from about 6 μm to 20 μm. The observation window (right) is 106.63 × 106.63 μm. The bleaching time τ_b has been varied with a maximum value of 480 ms.

and illuminates a small portion of the observation field as shown in Fig. 1. Since we only focus here on 2D velocimetry, we chose for the bleached region a rectangular zone oriented along the x-axis, perpendicular to both the flow direction (y) and the velocity gradient (z). Two parameters could be easily varied: the width of the bleaching line, and the duration of the bleaching step. Just after this step the imaging sequence starts, in which the laser intensity is lowered at about 70% of the maximum intensity.

The experiment requires the bleaching to be highly efficient to improve the signal to noise ratio. Indeed, as will be explained and illustrated in the following, on one hand the bleaching duration needs to be small in order to reduce the diffusion of the bleached dyes, and on the other hand the signal to noise ratio needs to be increased in order to be able to determine accurately the intensity profile. Optimal conditions for bleaching and illumination are thus required. For that purpose, we use aqueous solutions of fluorescein isothiocyanate (FITC) purchased from Sigma-Aldrich at a concentration of 0.1×10^{-3} mol L^{-1} and adjust the pH of the mixture to a value of 7 by adding some drops of NaOH. Within these conditions (and without flow), the fluorescence intensity drops approximately by a factor of 2 in 0.25 s, at the maximum laser power.

In order to characterize the bleaching resolution in the vorticity direction, we performed a vertical (z) scan of an immobile sample of fluorescein in a water–glycerol mixture at a mass ratio of 1 : 9, just after photobleaching a region aligned in the x direction at $z = 0$ μm (channel center) in a microchannel with $h = 100$ μm. The resulting fluorescence intensity is displayed in Fig. 2. The diffusion coefficient of fluorescein in this solution is on the order of 10^{-12} m^2 s^{-1}, so that the distance travelled due to diffusion is about 1 μm, given the experimental time scale. Thus the image reflects spatial variations of the photobleaching in the z direction due to the numerical aperture of the used objective. It is clear from this measurement that photobleaching is rather poorly resolved in the vertical direction, in contrast to the resolution in the focal plane. The typical decay of the photobleaching occurs at about 10 μm. When departing from the initial focal plane, the bleached line becomes smoother and wider reflecting the Gaussian beam of the laser with maximum intensity in the focal plane. An important consequence of this is the fact that we can assume in a first approximation that the photobleaching is independent of z, providing that vertical displacements within the experimental time scale are also smaller than 10 μm and by choosing the minimum pinhole for the confocal measurements.

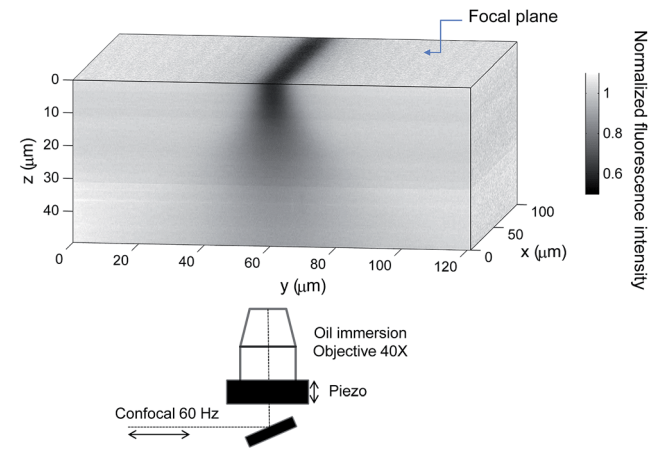

Fig. 2 Experimental determination of the Rayleigh collimated range in a microchannel of $h = 100$ μm filled with a fluid having a viscosity approaching the viscosity of glycerol in order to minimize the effect of molecular diffusion. The 3D imaging has been performed after bleaching a 6 μm rectangular band at $z = 0$ μm and then imaging half-channel while the fluid is at rest. In order to have a clear view of the bleaching depth the bleaching time has been set to $\tau_b = 0.73$ seconds. The depth of the photobleached region is about 10 μm. For symmetry, in the picture is shown half of the total channel height.

3 Intensity curve analysis

3.1 Intensity curve measurements

We focus in this paper on flows that are invariant in the x-direction (see Fig. 1). This allows to increase of the signal to noise ratio by averaging the image along x. The resulting intensity curves $I(y)$ are however not uniform, even without bleaching, and their shapes depend on the flow rate and optical conditions. This is mainly due to the progressive bleaching of the solution, which occurs even with the low intensity laser power used for the observation. Without flow, the intensity decreases slightly with time. As soon as the flow is set, the image reaches rapidly a steady state exhibiting an intensity gradient, in the opposite direction to that of the flow. In order to suppress this effect, we systematically acquire a reference image $I_0(y)$, with the same imaging parameters as the image sequence used for the velocity measurement. Then the corresponding reference image $I_0(y)$ (image before bleaching) is systematically used to normalize each one of the bleached sequence. In the following, we define as "intensity" the quantity $(I_0 - I)/I_0$. The intensity vanishes when the bleached molecule concentration is much smaller than the total dye concentration, and this is a monotonic function of the bleached molecule concentration. For the laser power used and the fluorescein concentration, we have verified that the relationship between $(I_0 - I)/I_0$ and the bleached dye concentration is linear.[22]

Fig. 3 shows examples of the resulting intensity profiles for different microflow conditions. Depending on the experimental parameters (fluid velocity and viscosity, bleaching width w_b and duration τ_b), these profiles can exhibit various shapes, which might be classified into three categories, as illustrated in Fig. 3. The profiles are often Gaussian-like (see *e.g.* Fig. 3, top). The symmetry reveals an equilibrium between convection and diffusion. By increasing the velocity (or by increasing the bleaching duration), they become asymmetric, long-tailed in the flow direction, denoting an increase of convection with respect to molecular diffusion. When increasing the fluid viscosity at small velocities, the longer tail switches to the opposite side (see Fig. 3, bottom) and the curves try to maintain the shape of the rectangular source. We propose in the following an analysis aiming to describe these shapes, to extract

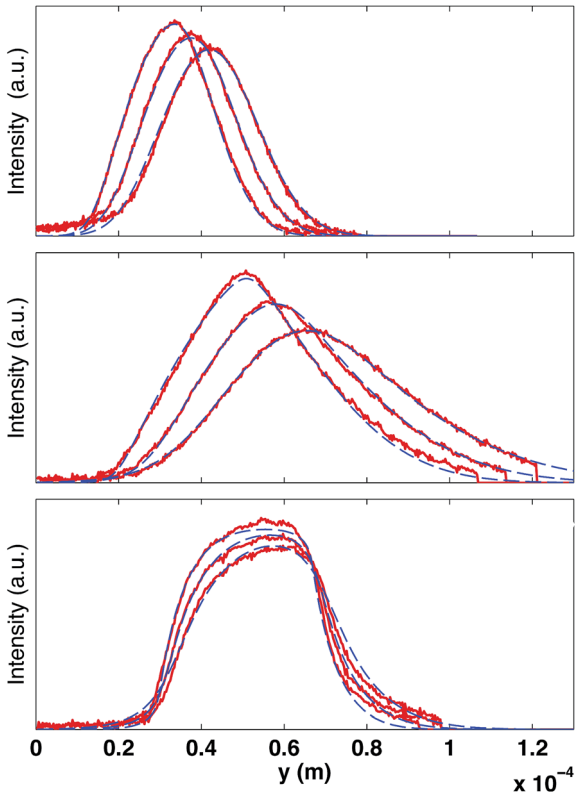

Fig. 3 Examples of intensity curves in the observation window after photobleaching for different experimental conditions. The signals are obtained by row-averaging in the x-direction and after normalizing by the background signal (image before bleaching). The solid lines are the experimental data (displayed each 116 ms) while the dash-dotted curves are the best fits to the experimental data, by using eqn (8) and (9). The fitting parameters are the velocity $v(z_0)$, the local shear rate $\dot{\gamma}$ and the curve center x_0. (Top) Gaussian-like profiles obtained at $\Delta P =$ 0.8 mbar with a fluid of viscosity of $\eta = 0.0059$ Pa s ($D = 7.1 \times 10^{-11}$ m^2 s^{-1}); bleaching parameters: $\tau_b = 0.32$ s, $w_b = 11$ μm; fitting parameters $v = 40$ μm s^{-1}, $\dot{\gamma} \simeq 0$. (Middle) Asymmetric triangular profiles are obtained by increasing the applied pressure to $\Delta P = 2.4$ mbar, and increasing the bleaching time and width ($\tau_b = 0.5$ s, $w_b = 18$ μm); fitting parameters $v = 77$ μm s^{-1}, $\dot{\gamma} = 6.6$ s^{-1}. (Bottom) Increasing the viscosity to $\eta = 0.0388$ Pa s ($D = 1.1 \times 10^{-11}$ m^2 s^{-1}), the profiles become asymmetric with the maximum value shifted toward the flow direction; bleaching parameters: $\tau_b = 0.5$ s, $w_b = 18$ μm; fitting parameters $y = 16$ μm s^{-1}, $\dot{\gamma} = 9.6$ s^{-1}.

from their dynamics the local fluid velocity to reconstruct the 2D velocity profiles.

3.2 Theoretical analysis of the intensity measurements

Let us consider the transport properties of the bleached molecules in a pressure driven flow in parallel plate geometry. The velocity v is aligned with the y-direction, parallel to the plates, and the velocity gradient is perpendicular along the z direction. The concentration field $c(y, z)$ of the bleached molecules is solution of the convection–diffusion equation:

$$\frac{\partial c}{\partial t} + v(z)\,\frac{\partial c}{\partial y} = D\Delta c + s \qquad (1)$$

with, as boundary conditions, no flux at the channel walls and a vanishing concentration at infinity. In the previous equation, D is the molecular diffusion coefficient and s is a source term corresponding to the bleaching process. For the plane Poiseuille flows in channels of height h considered in this study, the velocity along the z-axis is $v(z) = U(1 - 4z^2/h^2)$.

As shown in the previous section, the bleaching efficiency is maximal in the focal plane but only slightly decreases when moving along the z-direction. Therefore, as a first-order approximation, we could assume the source term s to be independent of z. As will be detailed in the following, we cannot neglect the finite duration and the finite width of the bleaching process. The solution of eqn (1) corresponding to the real source term could be easily derived by convolving the latter with the impulse response, *i.e.* when s is a simple pulse in time and in the flow direction. We will thus first focus on the Green function of the problem, c^0, before proceeding with its convolution. This situation corresponds to the classical dispersion phenomenon in Poiseuille flows, first studied by Taylor[25] and Aris,[26] and then refined and generalized by tens of authors due to its practical importance in many fields, including analytical chemistry. For the velocimetry application that is the purpose of this work, we need to focus on the short time response as the asymptotic concentration profile at long times is independent of z. Unfortunately there is no simple analytical solution available at all times, so we will use a numerical solution.

A simple way to compute it is to solve the corresponding stochastic equation. For this purpose, we consider 10^5 tracer particles homogeneously distributed in the z direction. The particles are launched at $t = 0$ from position $y = 0$. The particles are convected by the flow and diffuse randomly; their positions $\vec{r}_i(t)$ are computed according to:

$$\vec{r}_i(t + \delta t) = \vec{r}_i(t) + v(z)\delta t\vec{e}_y + 2\sqrt{D\delta t}\vec{\omega}_i, \qquad (2)$$

where $\vec{\omega}_i$ is a unit vector with a random direction in the plane $(\vec{e}_y, \vec{e}_z)$. Fig. 4 displays the evolution of the concentration field in dimensionless coordinates ($\tilde{y} = 2y/h$, $\tilde{z} = 2z/h$, $\tilde{t} = t2U/h$) for a Peclet number Pe $= Uh/D = 133$. At the short and moderate times displayed, the concentration field reflects roughly the parabolic profile of the velocity. We note however that close to the wall, the maximum of the concentration does not remain immobile as it would be the case in the absence of shear and diffusion. We will come back to this point later.

From the experimental intensity profiles and using the above detailed numerical approach, one could use an inverse method to deduce the velocity profile. However, this strategy is time

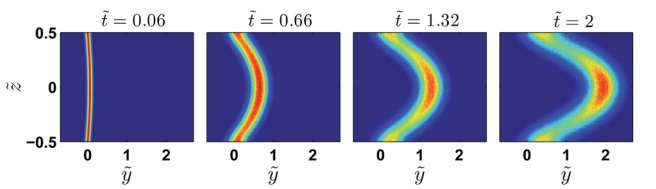

Fig. 4 Numerical solutions of the Green function of eqn (1), for Pe = 133 at $\tilde{t} = 0.06$, 0.66, 1.32 and 2.

consuming and we propose in the following a more direct and robust approach to obtain the velocity field, based on an approximate analytical solution.

Let us recall the main features of the classical dispersion problem of diffusing probes in pipe flow or in between parallel plates. Three regimes of spreading of a very thin line could be distinguished.[27] At very short times, for $t \ll h^{4/3}U^{2/3}/D^{1/3}$ (*i.e.* $\tilde{t} \ll \mathrm{Pe}^{1/3}$), dispersion due to molecular diffusion dominates over the effect of shear. The probes are convected according to the velocity profile and the line width scales as $\sigma = \sqrt{Dt}$. At longer times, but before the characteristic time to diffuse along the whole thickness $\tau_d = h^2/D$ (*i.e.* $\mathrm{Pe}^{1/3} \ll \tilde{t} \ll \mathrm{Pe}$), the dispersion is due to the combination of transverse diffusion and longitudinal shear. In this regime of so-called anomalous diffusion,[28] the dispersion increases more rapidly with time, and scales as $UD^{1/2}t^{3/2}/h$. The well-known Taylor dispersion only occurs at long times, *i.e.* for $t \gg \tau_D$. Clearly, this regime is not interesting for velocimetry applications since the diffusion process homogenizes the concentration along the thickness, and the traveling velocity of the bleached line equals the mean value of the velocity field, as in the case of ref. 22 where the considered thicknesses were smaller than a few micrometers. Note that in channel flows, a fourth regime exists at longer times,[29] for $t \gg w^2/D$, where hydrodynamic dispersion along the channel width takes place. There is no need to consider it in this study and we can model the flow geometry by two infinite parallel plates.

For the experiments presented here, τ_d is always greater than 25 s for the solutions studied (diffusion coefficient of fluorescein of 4×10^{-10} m^2 s^{-1} in water[30]), whereas the experiment duration is less than 1 s. We thus focus on the solution of the convection–diffusion equation in the diffusive and anomalous regime, where the characteristic transverse distance traveled by the tracers is much smaller than the channel thickness. In our experiments, the concentration profile is measured in the focal plane, located at z_0. It is then convenient to rewrite eqn (1) in the moving frame $v(z_0)$, and in the vicinity of the observation plane

$$\frac{\partial c}{\partial t} + (z - z_0)\dot{\gamma}(z_0)\frac{\partial c}{\partial y'} = D\Delta c + s \tag{3}$$

where $y' = y - v(z_0)t$ and $\dot{\gamma}$ is the velocity gradient at $z = z_0$. Note that we only keep the first term of Taylor expansion of the velocity field since the transverse displacement due to diffusion remains small.

The impulse response of eqn (3) is given by:[31]

$$c^0(y', t) = \frac{H(t)}{\sqrt{4\pi D_{\mathrm{eff}}(t)t}} \exp\left[-\frac{y'^2}{4D_{\mathrm{eff}}(t)t}\right], \tag{4}$$

where

$$D_{\mathrm{eff}}(t) = D\left(1 + \frac{1}{3}\dot{\gamma}^2 t^2\right) \tag{5}$$

and $H(t)$ is the heavyside function. This solution predicts that the concentration profiles are Gaussian functions at a given height $\tilde{z}$ centered at $v(z_0)$. Note that this solution is not valid close to the wall since the no-flux boundary condition is satisfied for $z = \pm\infty$ and not for $z = \pm h/2$. We can thus anticipate some deviations from this solution in the near-wall region, but also in the center where the first term of the Taylor expansion vanishes.

Fig. 5 shows examples of the concentration profiles corresponding to the numerical solution of eqn (1) and to the approximate analytical solution displayed eqn (4). The two sets of data agree quite well in the typical range of time scales corresponding to the experiments. Slight discrepancies are however evidenced close to the wall. The numerical simulation does not predict spreading in the negative $\tilde{y}$ region whereas the analytical formula does. To go further in the comparison of the two methods, we use the analytical expression to fit the numerical solution at fixed heights with effective dispersion coefficient D_{eff} and apparent velocity v_{app} as fitting parameters. The fits are excellent as the concentration profiles of the numerical solution are Gaussian-like for a given height. The difference between the local velocity and the best fit parameter v_{app} is shown in Fig. 5c. We note that it exists a discrepancy between the two sets of data in a thin region close to the wall which increases with time. The analytical approximate solution underestimates the longitudinal displacement in the vicinity of the wall and slightly overestimates it in the center of the channel. These differences are easily explained by considering the longitudinal transverse displacement due to molecular diffusion which averages the convective displacement on a distance on the order of $\sqrt{Dt}$. In the center of the gap, the

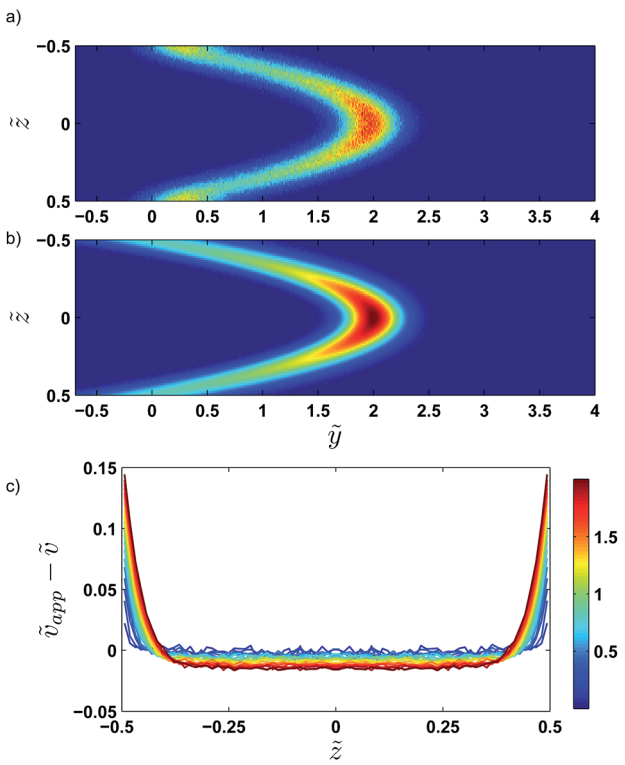

Fig. 5 Comparison between the numerical solution (a) and the approximate analytical solution (b), for Pe = 133 and $\tilde{t} = 2$. (c) Detailed comparison of the velocity profile $v(\tilde{z})$ and the apparent velocity v_{app}, obtained by fitting for each height $\tilde{z}$, the numerical solution with the approximate analytical one. Line colors are set according to time $\tilde{t}$ as indicated in the color bar.

difference between the two approaches is less than 1% of the maximal velocity so that we neglect it in the following. Close to the wall however it is worthwhile to quantify it. We have verified that the above scaling argument applies, *i.e.* the apparent velocity at the wall increases as $\dot{\gamma}\sqrt{Dt}$. More precisely, we find that it is within 1% given by

$$v_{\text{wall}} \simeq 2.56U\sqrt{Dt}/h. \quad (6)$$

Both the bleaching duration τ_b and spatial width w_b cannot be neglected since they are on the order of the acquisition time scale. From the approximate Green function c^0 displayed in eqn (4), the solution for an arbitrary source could be calculated using a convolution, which reads

$$c(y', z, t) = \int c^0(\lambda, \tau)s(y' + v_0(t-\tau) - \lambda, t-\tau)\mathrm{d}\tau\mathrm{d}\lambda, \quad (7)$$

We assume that the source s is given by $s(y, t) = s_0 \sqcap(y/w_b) \sqcap(t/\tau_b)$, where $\sqcap$ is the rectangular function. We obtain for $t > \tau_b/2$:

$$c(y, z_0, t) = c_0 \int_{t-\tau_b/2}^{t+\tau_b/2} [\psi(w_b, \tau) - \psi(-w_b, \tau)]\mathrm{d}\tau, \quad (8)$$

where

$$\psi(w_b, \tau) = \mathrm{erf}\left[\frac{w_b/2 + y - v(z_0)\tau}{\sqrt{4D\tau(1+\tau^2\dot{\gamma}^2/3)}}\right]. \quad (9)$$

Eqn (8) and (9) are of great practical interest since we could use them directly to fit the experimental intensity profiles, and to extract the apparent velocity. In order to obtain a robust fitting procedure, we proceed as follows. For a given height z_0, the whole time series of 15 images is fitted simultaneously, with the local velocity v_0, the shear rate $\dot{\gamma}$ and the constant c_0 as fitting parameters. Examples of the resulting intensity profiles are displayed in Fig. 3. The good agreement obtained shows that the assumption of a rectangular source term both in time and in space is valid, and validates the method. It is worth noting that the model accounts well for the asymmetric shapes of the intensity curves. We also find that the fitting procedure is rather sensitive to the diffusion coefficient, and it would also be possible to deduce it from the experiments. The value of the molecular diffusion coefficient set in our fitting procedure was calculated assuming that $D = D_w\eta_w/\eta$, where η is the liquid viscosity, D_w is the fluorescein diffusion coefficient in water (4×10^{-10} m^2 s^{-1}, according to ref. 30), and η_w the water viscosity.

To conclude this section, two additional comments should be made.

First, we recall that the above solution is only valid for $t \ll \tau_d$. At longer times, the transverse displacement would be large and the modeling of the velocity field by a single local shear rate (see eqn (3)) would not be valid. In principle, one should also include an extra term in the Taylor expansion in the center of the channel since the shear rate vanishes, but profiles acquired in this region still show good agreement with the proposed model. Furthermore the influence of the no-flux boundary conditions at the wall would at longer times affects the whole concentration field.

Second, although the impulse response (eqn (4)) exhibits a maximum at $y = v(z_0)t$, this is generally not true for a source of finite duration (eqn (8)). The corresponding solutions are asymmetric, and the curve shape evolves with the observation time. They eventually reach a Gaussian-like profile. Therefore, by looking simply at the displacement of the maxima of the intensity curves it would lead to systematic errors, whenever the profiles are non-symmetric.

4 Velocity measurements

In order to validate the proposed velocimetry method, we apply it on pressure-driven flows. We recorded videos of the flow at successive heights covering the whole channel depth. It is necessary to wait a few seconds between two bleaching steps at different z in order to ensure that bleached molecules have traveled out of the observation window. We apply this experimental procedure for two different channels with $h_1 = 50$ μm and $h_2 = 100$ μm and two different viscosities $\eta_1 = 0.0059$ Pa s and $\eta_2 = 0.0388$ Pa s by controlling accurately the inlet–outlet pressure ΔP. As discussed in the previous section, different families of intensity curves are obtained from experiments. The flow profiles are obtained by fitting simultaneously 15 experimental curves, captured at each focal plane and corresponding to an observation time of $\tau_0 = 0.25$ s, with eqn (8) and (9), and having the local velocity, shear rate, and curve center x_0 as fitting parameters. Fig. 6 displays the corresponding results in channels of heights 50 (top, Fig. 6) and 100 μm (bottom, Fig. 6). They are compared with the theoretical profiles, corresponding to Poiseuille flow, *i.e.* $v = U(1 - 4z^2/h^2)$, where $U = h^2\Delta P/8\eta L$. There are no fitting parameters; the viscosity η has been determined for the two fluids by using a cone–plate rheometer.

For the sets of experiments we calculate the velocity at the channel center. This procedure is rather easy because the intensity curves are almost Gaussian-like at $z_0 = 0$ and the dynamics of the intensity curves is not affected by the local shear rate $\dot{\gamma}$ as it will be explained in the following. In Fig. 7 the maximum velocity *versus* the applied pressure ΔP is shown.

From this graph we can conclude that the method is well suited to calculate the maximum velocity with and error below 1%. The limit in the maximum velocity calculation lies mainly on the acquisition frame rate and on the size of the observation window (space available to have at least two intensity curves) because the displacement of the profile becomes too fast to be monitored. We can conclude that, with our optical setup, the limit in the maximum velocity is about 485 μm s^{-1} (see light triangles in Fig. 7). It would be possible to extend the experiments to higher velocities by using an objective of lower magnification, but the confocal depth would then be higher, lowering the z-resolution of the transverse profile. As for the low velocity limit, the band displacement would become too small as compared to the line diffusion. We did not test this low velocity limit in this work, but since dispersion due to shear is in this case negligible, it is possible to refer to our previous

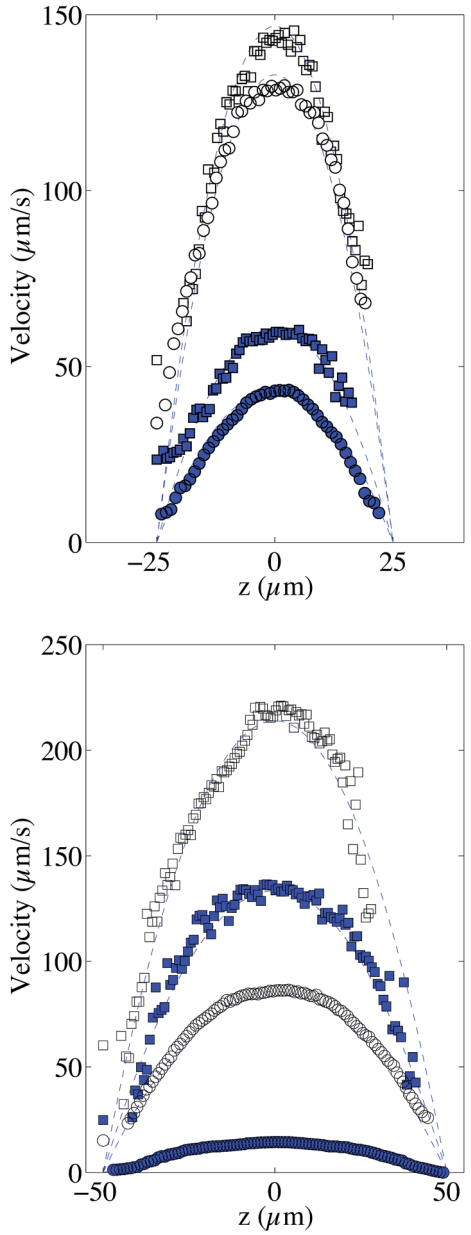

Fig. 6 Comparison between measured velocity profiles and theoretical prediction of the Poiseuille flow (dashed lines) for different applied pressure (top) $\Delta P = 2.8$ mbar (light squares), $\Delta P = 1.1$ mbar (full squares), $\Delta P = 16.4$ mbar (light circles) and $\Delta P = 5.4$ mbar (full circles) in a $h = 50$ μm microchannel with a fluid having a viscosity of $\eta = 0.0059$ Pa s (squares) and $\eta = 0.0388$ (circles). (Bottom) $\Delta P = 1$ mbar (light squares), $\Delta P = 0.6$ mbar (full squares), $\Delta P = 2.6$ mbar (light circles) and $\Delta P = 0.4$ mbar (full circles) in a $h = 100$ μm microchannel. The viscosity of the fluid is $\eta = 0.0059$ Pa s (squares, $D = 7.1 \times 10^{-11}$ m^2 s^{-1}) and $\eta = 0.0388$ (circles, $D = 1.07 \times 10^{-11}$ m^2 s^{-1}).

work,[22] where velocities as low as 0.1 μm s^{-1} were reported. Coming back to the reconstructed velocity profiles, it is however clear from the profiles in Fig. 6 that there is a deviation between experimental and theoretical profiles close to the walls. The experimental results overestimate the theoretical velocity at the walls and this overestimation is proportional to the maximum velocity (see Fig. 8). Since we do not expect at these length scales

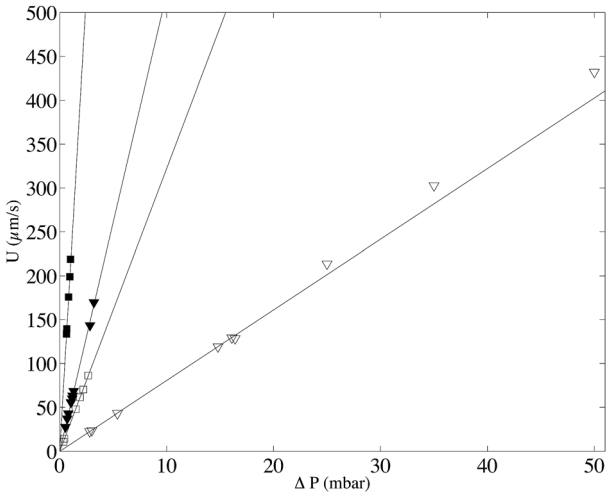

Fig. 7 Maximum velocity U *versus* the applied pressure. The lines correspond to the theoretical values while symbols correspond to the values calculated from experiments for a $h = 50$ μm microchannel with a fluid having a viscosity of $\eta = 0.0059$ Pa s (full triangles) and $\eta = 0.0388$ Pa s (light triangles); for a $h = 100$ μm microchannel with a fluid having a viscosity of $\eta = 0.0059$ Pa s (full squares) and $\eta = 0.0388$ Pa s (light squares).

any deviations from the Poiseuille law, there is a bias coming from the experimental technique itself. For the experimental conditions of the data reported in Fig. 6, the near-wall region

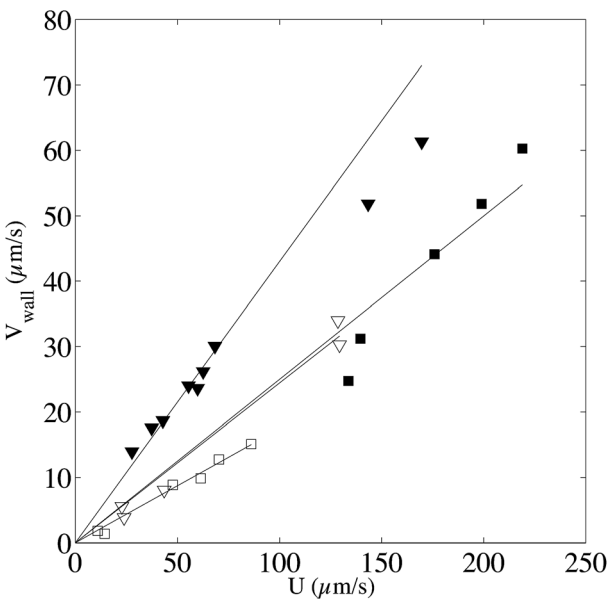

Fig. 8 Apparent velocity measured at the wall as a function of the maximum velocity U for a $h = 50$ μm microchannel with a fluid having a viscosity of $\eta = 0.0059$ Pa s (full triangles) and $\eta = 0.0388$ Pa s (light triangles); for a $h = 100$ μm microchannel with a fluid having a viscosity of $\eta = 0.0059$ Pa s (full squares) and $\eta = 0.0388$ Pa s (light squares). The lines are the best linear fit of slope 0.17 (light squares), 0.24 (light triangles), 0.25 (full squares) and 0.43 (full triangles). We expect (see text) that $v_{\text{wall}} \simeq 2.56\sqrt{D\tau}/h \times U$. The theoretical values (0.1, 0.198, 0.27, 0.57) are in general in good agreement with the experimental values.

represents a maximum value of about 5 μm at the lower viscosity value. As detailed in the previous section, the theoretical predictions are not valid near the walls, since the used solution does not respect the no-flux boundary conditions at the wall. In the data displayed in Fig. 6, the experimental time τ, which is the sum of the bleaching time and the observation time, is about 0.5 s, and the local shear rates on the order of 1 s^{-1}, so the $|\dot{\gamma}|\tau$ is on the order of unity. Therefore, in eqn (9), it is not possible to neglect the advection term due to the local shear rate. During the experimental time, the transverse displacement due to diffusion is given by $\sqrt{D\tau}$. Therefore, in the plane located in z_0, the bleached molecules observed at time τ have explored by diffusion a layer of height $\sqrt{D\tau}$ centered at z_0. Due to local shear, there is thus an additional displacement in the flow direction of the order of $\dot{\gamma}D^{1/2}\tau^{3/2}$. In a simple shear flow and away from the wall, it is straightforward by symmetry that this displacement does not have any consequences on the mean displacement. Only the spreading is affected, as captured in the analysis, eqn (5). However, the wall breaks the vertical symmetry, and the additional positive displacement due to the local shear is not counterbalanced in the vicinity of the solid surface. Therefore, the velocity is overestimated in a near-wall region of extent $\sqrt{D\tau}$, by a quantity $\dot{\gamma}\sqrt{D\tau}$. As a practical consequence, the overestimation of the velocity near the wall could be smaller by reducing the experimental time or by decreasing the diffusion D of molecules thus increasing the fluid viscosity. This is checked in Fig. 9, where the apparent measured wall velocities normalized by the maximum velocity U and plotted *versus* $\sqrt{D\tau}/h$ are reported. The spreading of the points for fixed $\sqrt{D\tau}/h$ in the vertical direction is due to the increase of $\dot{\gamma}$ with the imposed pressure gradient. The scaling is well captured for the size of channels and viscosities of fluids tested. In fact, looking for prefactors, we obtain quantitative agreement for the data displayed in Fig. 8. In Fig. 9 the normalized apparent velocity at the wall is shown from lower to higher diffusion rate and is equal to $2.2\sqrt{D\tau}/h + 0.10$. From numerical simulations, we expect (see text in Section 3.2) that $v_{\text{wall}} \simeq 2.56\sqrt{D\tau}/h \times U$.

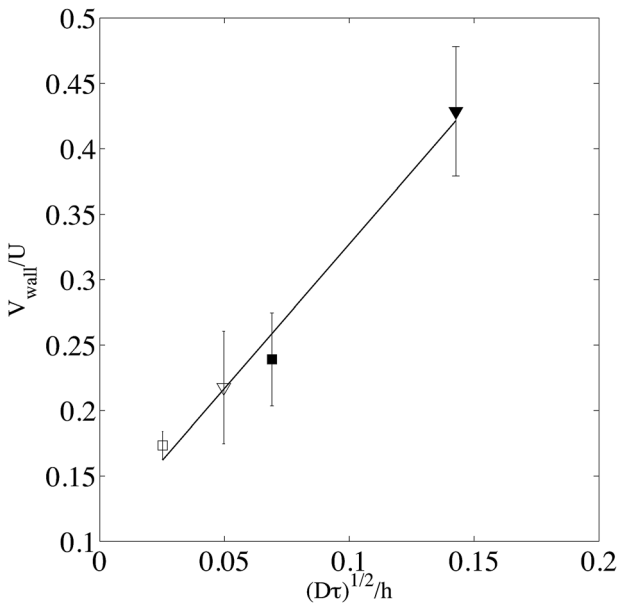

Fig. 9 Measured velocity at the wall normalized by the maximum velocity U and plotted as a function of $\sqrt{D\tau}/h$, where τ is the total experimental time $\tau = \tau_b + \tau_0$; τ_0 is the observation time, on the order of 0.23 s while τ_b can be varied (from 0.38 s to 0.48 s) according to the experiment. The best linear fit is $2.2\sqrt{D\tau}/h + 0.10$. Light and full symbols denote respectively higher (η = 0.0388 Pa s) and smaller viscosities (η = 0.0059 Pa s). Squares indicate a channel thickness h = 100 μm and triangles h = 50 μm.

We can thus conclude that using the proposed model, detailed in the previous section, we have validated the velocimetry technique using pressure-driven flows. It is precise and robust, but can lead to a systematic error near the wall, in a layer which extend for a maximum of 5 μm from the solid surface for dye of high diffusion coefficient in a low viscous fluid. Although it does not seem possible to lower this error, it is however possible to improve it by decreasing the observation time. Indeed, the layer where the velocity is overestimated is on the order of $\sqrt{D\tau}$.

The velocity range accessibility is limited in the low speed limit by the dye molecular diffusion. The displacement due to diffusion should be not too large as compared to advection. With FITC in water, the minimum measurable velocity is about a few micrometers per second.[22] The high speed limit comes from the scanning speed of the confocal microscope and from the image size related to the objective. For the conditions used in this work, this corresponds to 1 mm s^{-1}. This high speed limit could be increased by using an objective of lower magnification. It is important to mention that the bleached line displacement between two successive images should be low enough to be able to neglect the disturbance caused by the scanning nature of confocal microscopy, or alternatively, to correct the apparent displacement.[32]

As compared to PTV and PIV methods, photobleaching under flow remains limited to uni-dimensional flows, although extensions to 2D are in principle possible using a bleached spot instead of a bleached line. Due to smaller diffusion coefficient, these particle-based velocimetry techniques do not suffer directly from the wall effect discussed above, but also exhibit a bias on a length scale on the order of the particle size, similar to the overestimation near the wall of the presented method.

5 Application to complex flows

As explained in the Introduction, the main interest of the present technique lies on the use of molecular tracers, which do not perturb the flow and allow particle-fluid velocity measurements. Many complex fluids contain rather large objects on the order of tens of microns in diameter that could be observed using confocal microscopy. In this case, the technique presented in this paper could be of great interest, because it is possible to measure simultaneously the fluid velocity together with the observation of particle trajectories.

As an illustration of such a possibility, we disperse PMMA particles (spheromers CA6, purchased from Microbeads) in a mixture of thioglycerol and deionized water (4 : 1 weight fraction) containing fluorescein at 0.1 × 10^{-3} mol L^{-1}. The

suspension is both buoyancy and refractive index matched. Two suspensions at different volume fractions (0.11 and 0.53) are flowed in our device ($h = 50$ μm), and the suspending fluid velocity is characterized thanks to photobleaching experiments. Since the particles appear in black on the images (see examples displayed in Fig. 10), we first segmented the particles in each image to create a mask so that we can focus only on particle-free regions to determine the fluid velocity minimizing the noise due to the black particles. At the same time we locate the particles and subsequently we measure the mean velocity using a standard tracking algorithm.[8] For the fluid velocity measurement, we use exactly the same procedure described in Section 3 deducing the velocity of the liquid phase in each focal plane through the channel depth.

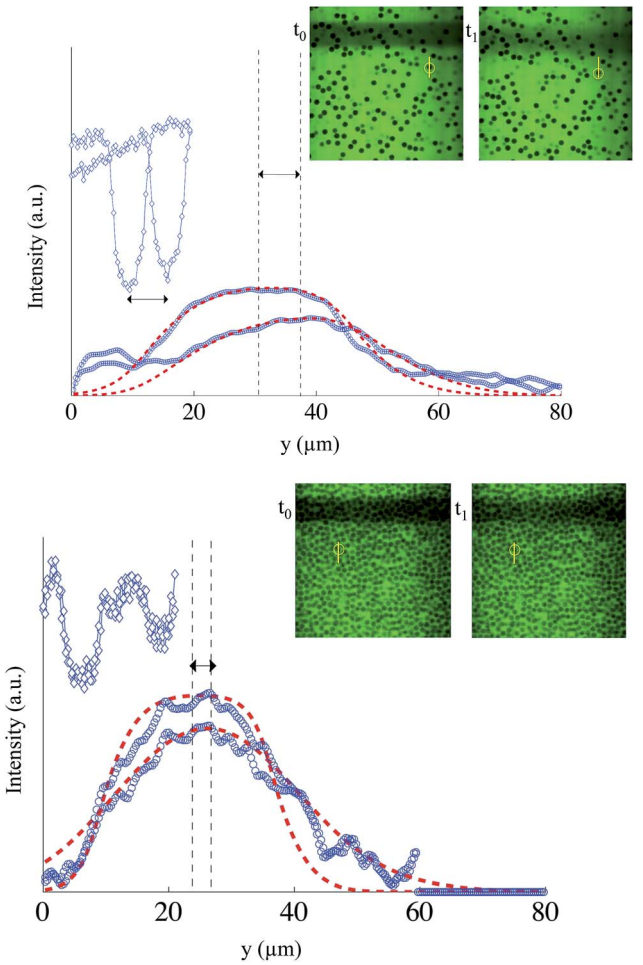

Fig. 10 Illustration of the simultaneous measurement of liquid and particle velocity for a suspension of 6 μm diameter PMMA particles in a mixture of thioglycerol and water (density and refractive index matched), flowing in a 50 μm thick microchannel. The local particle volume fraction is 0.11 (top) and 0.61 (bottom). The liquid velocity is estimated from the displacement of the photo-bleached line, by fitting (dashed lines) the intensity curves (light circles) of the particle free region. The experimental intensity curves related to the fluid displacement are displayed in the graphs as circles for two different times $t_0 = 0$ (reference bleaching time) and $t_1 = 0.33$ s (top) and $t_1 = 0.51$ s (bottom). We found a fluid velocity of 20.2 μm s^{-1} in the first case (top), and 5.7 μm s^{-1} in the second one (bottom). The solid line with rhombuses represents the intensity profile along the green line shown on the images, and shows the displacement of a particle by looking at the location of the minimum. The selected particles are evidenced by a circle on the images. The mean velocity of the particles, determined by μ-PTV, is 19.7 μm s^{-1} in the first (top) case, and 0.017 μm s^{-1} in the second case.

Fig. 10 shows two different examples of velocity measurements. In the first example (see Fig. 10, top), we imaged a plane located at $z_0 = -17$ μm where the local particle volume fraction of 0.11 is rather low and the liquid velocity is found to be 20.2 μm s^{-1} while the mean particle velocity calculated by means of PTV is 19.7 μm s^{-1} with a standard deviation of 0.8 μm s^{-1}. Thus, in this case the fluid and particle velocity could be considered the same.

By increasing the volume fraction of the suspension to 0.53, we observe a partial clogging of the channel due to particle accumulation. The local volume fraction reaches a value of 0.61 (see Fig. 10, bottom). Friction forces between particles are able, at this stage, to balance the drag force, so that the particle velocity is almost zero. It is much lower than the liquid velocity, estimated in this example to be 5.7 μm s^{-1} thanks to the photobleaching procedure. This state is not very different from the flow of a liquid in a porous medium made of solid particles. In this case, and whenever there exists a velocity difference between the fluid and the particles, the wall effect discussed in the previous section prevents an accurate spatial resolution of the velocity between arrested particles. Only the mean velocity difference can be measured given the small distance between particles.

These two examples show that the technique presented here is adequate to measure velocity differences between small scale particles and their suspending liquid in microfluidic devices. As explained in the introduction, this has some direct applications for lab-scale studies of flow properties of concentrated suspensions. Moreover, the presented velocimetry technique could also be useful for studies focusing on emulsions, transport properties in porous systems, extrusion processes of microparticulate paste where liquid maldistribution[33] and liquid phase migration[34] has been found to play a major role in the final product properties.

6 Conclusion

In conclusion, we have studied the possibility of using confocal microscopy and photobleaching under flow as a velocimetry technique in microchannels. The method basically consists of following the displacement in time of bleached molecules at different focal planes through the channel depth. Despite this apparent simplicity, it is not straightforward as the resulting intensity curves could be asymmetric depending on the bleaching conditions and on the importance of convection and diffusion effects, together with the finite duration and width of the bleaching. We provide a fast method to account for this effect based on the convolution of approximate analytical solutions of the convection–diffusion equation. For pressure-driven flows, the measurement is rather accurate, and validated

using various channel heights, liquid viscosities and pressure drops.

The main limitation of this technique comes from wall effects. Due to diffusion and in the presence of a solid surface, the velocity is overestimated in the vicinity of the wall. This drawback is typically important in a 5 μm layer for the lower viscosity considered in this study. The only possibility to reduce this effect is to decrease the duration of the bleaching or the diffusion coefficient. Although the first one is in principle feasible but limited by the signal to noise ratio, the second one would remove the main advantage of the presented technique which relies on the use of small molecular dyes as tracers.

Applications of this technique concern any flows which could be perturbed by tracer particles. For example, we have applied it to flows of suspensions below and above the jamming, and we have proved the possibility of measuring simultaneously the particle and liquid velocity. We restrict ourselves in this study to flows that are invariant in the vorticity direction, and we use for that purpose a bleaching region which is a band aligned to this direction. However, the extension of this technique to fully 3-D flow profiles is rather straightforward, but would require from an experimental point of view an increase of the signal to noise ratio, since it is not possible to benefit from the light intensity average in the vorticity direction. In a steady flow, this could be achieved by repeating a few times the experiments.

References

1 C. W. Macosko and J. Mewis, *Suspension Rheology*, VCH, 1994.
2 J. J. Stickel and R. L. Powell, *Annu. Rev. Fluid Mech.*, 2005, **37**, 129–149.
3 G. Ovarlez, F. Bertrand and S. Rodts, *J. Rheol.*, 2006, **50**, 259–292.
4 D. Lhuillier, *Phys. Fluids*, 2009, **21**, 023302.
5 J. G. Santiago, S. T. Wereley, C. D. Meinhart, D. J. Beebe and R. J. Adrian, *Exp. Fluids*, 1998, **25**, 316–319.
6 R. Lindken, M. Rossi, S. Große and J. Westerweel, *Lab Chip*, 2009, **9**, 2551–2567.
7 S. J. Lee and S. Kim, *Microfluid. Nanofluid.*, 2009, **6**, 577–588.
8 J. C. Crocker and D. G. Grier, *J. Colloid Interface Sci.*, 1996, **179**, 298–310.
9 J. Gelles, B. J. Schnapp and M. P. Sheetz, *Nature*, 1988, **331**, 450–453.
10 R. N. Ghosh and W. W. Webb, *Biophys. J.*, 1994, **66**, 1301–1318.
11 C. M. Anderson, G. N. Georgiou, I. Morrison, G. Stevenson and R. J. Cherry, *J. Cell Sci.*, 1992, **101**, 415–425.
12 D. Sinton, *Microfluid. Nanofluid.*, 2004, **1**, 2–21.
13 D. Ross, T. J. Johnson and L. E. Locascio, *Anal. Chem.*, 2001, **73**, 2509–2515.
14 J. P. Shelby and D. T. Chiu, *Anal. Chem.*, 2003, **75**, 1387–1392.
15 G. R. Wang, *Lab Chip*, 2005, **5**, 450–456.
16 G. R. Wang, I. Sas, H. Jiang, W. P. Janzen and C. Hodge, *Electrophoresis*, 2008, **29**, 1253–1263.
17 C. Kuang, W. Zhao, F. Yang and G. Wang, *Microfluid. Nanofluid.*, 2009, **7**, 509–517.
18 C. F. Kuang and G. R. Wang, *Lab Chip*, 2010, **10**, 240–245.
19 J. I. Molho, A. E. Herr, B. P. Mosier, J. G. Santiago, T. W. Kenny, R. A. Brennen, G. B. Gordon and B. Mohammadi, *Anal. Chem.*, 2001, **73**, 1350–1360.
20 B. Mosier, J. Molho and J. Santiago, *Exp. Fluids*, 2002, **33**, 545–554.
21 C. S. Garbe, *Pattern Recognit. Lect. Notes Comput. Sci.*, 2007, **4713**, 92–101.
22 A. Cuenca and H. Bodiguel, *Lab Chip*, 2012, **12**, 1672–1679.
23 A. Ponjavic, M. Chennaoui and J. S. Wong, *Tribol. Lett.*, 2013, **50**, 261–277.
24 J. Wexler, I. Jacobi and H. A. Stone, *66th Annual Meeting of the APS Division of Fluid Dynamics*, 2013.
25 G. I. Taylor, *Proc. R. Soc. London, Ser. A*, 1954, **67**, 857–869.
26 R. Aris, *Proc. R. Soc. London, Ser. A*, 1956, **235**, 67–77.
27 M. Latini and A. J. Bernoff, *J. Fluid Mech.*, 2001, **441**, 399–411.
28 M. J. Lighthill, *J. Inst. Math. Its Appl.*, 1966, **2**, 97–108.
29 A. Ajdari, N. Bontoux and H. A. Stone, *Anal. Chem.*, 2006, **78**, 387–392.
30 K. Pappaert, J. Biesemans, D. Clicq, S. Vankrunkelsven and G. Desmet, *Lab Chip*, 2005, **5**, 1104–1110.
31 P. B. Rhines and W. R. Young, *J. Fluid Mech.*, 1983, **133**, 133–145.
32 P. Jop, V. Mansard, P. Chaudhuri, L. Bocquet and A. Colin, *Phys. Rev. Lett.*, 2012, **108**, 148301.
33 A. Yu, J. Bridgwater, A. Burbidge and Z. Saracevic, *Powder Technol.*, 1999, **103**, 103–109.
34 S. Rough, J. Bridgwater and D. Wilson, *Int. J. Pharm.*, 2000, **204**, 117–126.